IEEE Access
Multidisciplinary | Rapid Review | Open Access Journal

Received June 27, 2020, accepted August 7, 2020, date of publication August 14, 2020, date of current version August 25, 2020.

Digital Object Identifier 10.1109/ACCESS.2020.3016726

Dynamic Modeling and Motion Control of a Cable-Driven Robotic Exoskeleton With Pneumatic Artificial Muscle Actuators

CHUN-TA CHEN, WEI-YUAN LIEN, CHUN-TING CHEN, MING-JENQ TWU, AND YU-CHENG WU

Department of Mechatronic Engineering, National Taiwan Normal University, Taipei 10610, Taiwan

Corresponding authors: Chun-Ta Chen (chenct@ntnu.edu.tw) and Yu-Cheng Wu (bihwa00191@gmail.com)

This work was supported in part by the Ministry of Science and Technology of Taiwan, under Contract MOST 108-2321-B-027-001 and Contract MOST 108-2221-E-003 -024-MY3.

ABSTRACT This paper presents the design, dynamic modeling and motion control of a novel cable-driven upper limb robotic exoskeleton for a rehabilitation exercising. The proposed four degree-of-freedom robotic exoskeleton, actuated by pneumatic artificial muscle actuators, is characterized by a safe, compact, and lightweight structure, complying with the motion of an upper limb as close as possible. In order to perform a passive rehabilitation exercise, the dynamic models were developed by the Lagrange formulation in terms of quasi coordinates combined with the virtual work principle, and then the adaptive fuzzy sliding mode control was designed for the rehabilitation trajectory control. Finally, rehabilitation experiments were conducted to validate the prototype of upper limb robotic exoskeleton and the controller design.

INDEX TERMS
Pneumatic artificial muscle, robotic exoskeleton, rehabilitation, adaptive fuzzy sliding mode control.

I. INTRODUCTION

Rehabilitation treatment, typically performed by caregivers and therapists, needs repeated and progressive functional training exercises to help impaired patients to recover motor abilities [1]–[3]. However, conventional therapist-led rehabilitation treatments require intensive labor, and typically are time-consuming [4]. With current robotic technique emerging, robots have been applied to diverse fields. Robotic devices have demonstrated the consistency in repetitive tasks. They are well suited for rehabilitation assistance [5]. In particular, end-effector-type manipulators have been used in the upper limb rehabilitation training to assist both therapists and the impaired to improve treatment [6], [7]. However, the heavy and stationary structures of these manipulators restrict the availability in the settings.

A robotic exoskeleton is a mechanical structure type of device whose joints and links are compatible with those of the human body [8]. The wearable characteristics of robotic exoskeletons offer potential applications to the rehabilitation assistances or powered assistances, and thus have gained more interests in robotic exoskeleton development [9]. In general, the designs on exoskeleton systems for upper-limb rehabilitation can be classified into the shoulder–elbow–wrist motion, shoulder–elbow motion and elbow–wrist motion [10]. In the supported motion of shoulder–elbow, research groups have designed various serial types of robotic exoskeletons for rehabilitation investigations like ALEx [11], CINVESRobot-1 [12], and AssistOn-SE [13]. While inspired by the human anatomy, the shoulder joint in our developed 4-DOFs of robotic exoskeleton for supported shoulder–elbow motion is a ball-socket joint.

Regularly, a user wears a robotic exoskeleton to undergo rehabilitation trainings, the exoskeleton has to convey forces to drive an upper arm to track the planed rehabilitation trajectory slowly, smoothly and safely [14]. Therefore, the mechanical design and control technologies of a robotic exoskeleton must play a critical role on the rehabilitation effects.

For electric-motor-actuated robotic exoskeletons, different mechanical designs and control strategies [15]–[18] have been proposed to conduct rehabilitation trainings by achieving a passive trajectory tracking, but the weights of most exoskeletons are still considerable for a human to wear. In comparison to the electric motors, pneumatic artificial

The associate editor coordinating the review of this manuscript and approving it for publication was Long Cheng.

muscles (PAMs) have several advantages like compactness, inherent compliance, low cost, and high power-to-weight ratio [19], [20]. PAM is a braided pneumatic actuator composed of an inner rubber tube wrapped in a layer of nonextendable double-helix-braided shell. When the tube is filled with air through a hose, the PAM contracts in the longitudinal direction according to its inflation volume, whereas it tends to return to its original shape during the deflation. These physical characteristics make PAMs become an alternative actuator.

In control technologies for PAM-actuated robotic exoskeletons, Andrikopoulos *et al.* [21] presented the design and motion implementation of a PAM-actuated 2-DOF wrist exoskeleton. Experimental evaluations on the movement capabilities were made via a PID-based control algorithm. A portable upper limb exoskeleton rehabilitation robot was developed by Tu *et al.* [22]. The rehabilitation robot was unidirectionally actuated by PAMs. The iterative learning control (ILC) was chosen to realize intensive and repetitive rehabilitation trainings. Xiong and Jiang [23] designed an exoskeleton robotic arm driven by PAMs for stroke rehabilitation. The patient-active-robot-passive and patient-passive-robot-active training modes were conducted by a PID control method.

Based on the aforementioned observations, linear type of controllers were most employed for the rehabilitation control of PAM-actuated upper-limb robotic exoskeletons. However, a linear type of controller is not enough for the better rehabilitation effects due to nonlinear phenomena of PAM-actuated systems that are resulted from air compressibility, friction, sensitivity to external loading, making control of a PAM-actuated exoskeleton rather difficult [24], [25]. Moreover, in order to improve the quality of the trajectory tracking of rehabilitation control, an advanced controller always needs the system dynamic models. However, the dynamic formulation is arduous for a complex system. Several methods such as the Newton-Euler formulation [26], [27], virtual work principle [28], [29], Kane's method [30], and the Lagrangian formulation in generalized coordinates [31]–[33] have been proposed for modeling and simulation of dynamic systems. Among them, the Lagrangian formulation based on the kinetic and potential energies has more physical insight. However, if the rotations of a structure in space are expressed in generalized coordinates, the formulated time-varying inertia matrices will lead to intensive symbolic computations for the partial derivatives of the Lagrangian, and thus the dynamic equations are developed only under some simplified assumptions on the geometry, configuration and inertia distribution. Instead, in the paper the Lagrange formulation in terms of quasi coordinates combined with the virtual work principle was proposed for the dynamic modeling of the robotic exoskeleton. The developed closed and complete dynamic equations are available for the model based control design.

In this paper, we depict a 4-DOF upper limb robotic exoskeleton design for the supported shoulder–elbow motion. The laboratory experimental robotic exoskeleton is actuated by PAMs through cables, and mainly serves as the passive rehabilitation mode. The passive rehabilitation assistance is achieved based on the trajectory tracking control. Due to the system uncertainties and external disturbances, the adaptive fuzzy sliding mode control (AFSMC) is proposed for the trajectory tracking of rehabilitation control. As aforementioned, the AFSMC needs the dynamic model, and thus the equations of motion were formulated using the Lagrange equations in terms of quasi coordinates combined with the virtual work principle, in which the formulated kinetic and potential energies are expressed in matrix forms as function of quasi-velocities and rotation matrices. Maneuvering tests on healthy subjects were implemented to validate the designed architectures and controllers for passive rehabilitation exercises.

The remainder of this paper is structured as follows: in section 2, the design and building of a four DOFs of PAMs-actuated robotic exoskeleton via cables is presented. Section 3 gives the complete dynamic formulation of the upper-limb robotic exoskeleton based on the Lagrange formulism in terms of quasi coordinates combined with the virtual work principle. Further, for the performance improvement on the rehabilitation trajectory tracking, the AFSMC design for the robotic exoskeleton is described in section 4. The stability proof is also provided here. In section 5, the rehabilitation trajectory tracking experiments are presented and discussed. Finally, brief conclusions about the contribution of this study are outlined in section 6.

II. DESIGN AND BUILDING OF ROBOTIC EXOSKELETON

A. OVERVIEW OF SYSTEM DESIGN

The design targets to develop a compact, light-weight upper limb robotic exoskeleton that fits to the anatomical structure and agrees with the movement of the upper limb as close as possible. In general, the human upper limb mainly consists of seven degrees of freedom, but most executed rehabilitation exercises involve shoulder abduction/adduction, shoulder flexion/extension, shoulder internal/external rotation, and elbow flexion/extension. As such, a four-DOF upper-limb robotic exoskeleton design is presented in this paper.

1) SHOULDER AND ELBOW JOINT DESIGN

As shown in Fig. 1(a) for the shoulder joint mechanism, the first L type of link is actuated through the ring bearing joint 1 that is mounted to the shoulder plate. The ring bearing joint 2 that is fixed to the first L type of link drives the second L type of link, and the housing cap for the upper arm support is rotated by the ring bearing joint 3. The length of the housing cap is varied by connecting a sliding link to adapt the different lengths of human arms. The proposed design, as shown in Fig. 1(b), emulates the anatomical ball-and-socket shoulder joints of human beings, and kinematically equivalent to a serial chain with three perpendicular revolute joint axes intersecting at a single point [34]. Moreover, the shoulder abduction/adduction θ_1, shoulder flexion/extension θ_2, and shoulder internal/external rotation θ_3 clearly agree

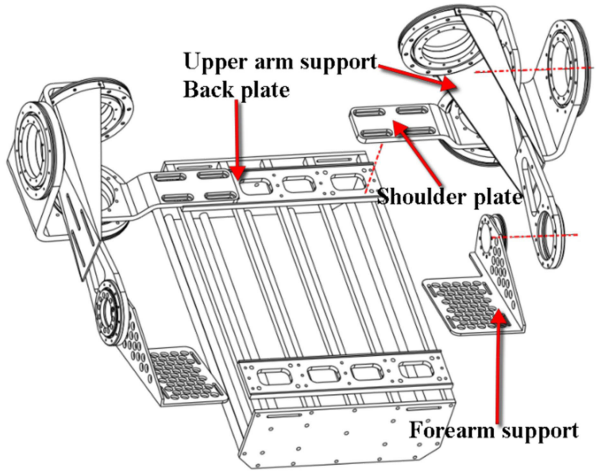

(a)

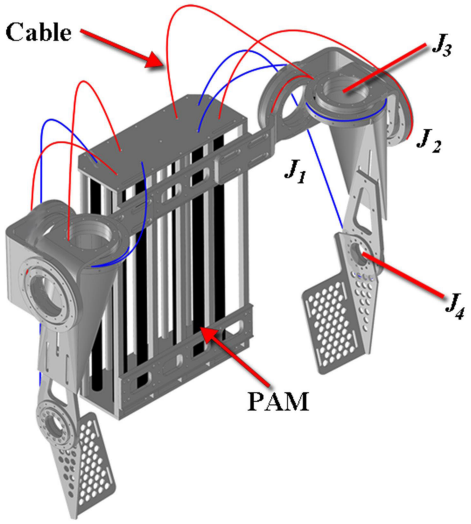

(b)

FIGURE 1. (a) Mechanical design of robotic exoskeleton for supported shoulder-elbow motion. (b) Joint configurations assignment.

with the description of the ZYX Euler angles for a coordinate system assignment.

In the elbow joint design, only allowed is the elbow flexion/extension θ_4. The forearm plate is therefore rotated by the inner ring shaft with an embedded bearing mounted to the support aluminum plate. Each joint is mounted with a high-resolution incremental encoder for the measurements of joint angles.

Coupling the free end of a PAM to each joint through a cable that is routed on the outer or inner ring axis generates a tension force or a contracting force as the air is compressed into the tube, and thus the revolute joint is actuated. The PAMs are Festo type MAS-20-300N fluidic muscles with the 25% maximum contraction ratio. A proportional pneumatic pressure regulator (Festo VPM-6L-L-1-G18-0L10H-V1N) is used to control the air into a PAM, and its pressure range is from 0 to 10 (bar) with respect to the input voltage. All the PAMs are directly placed on the backboard to achieve the compactness as well as decrease the whole weight of the robotic exoskeleton. Instead of imitating one pair of antagonist muscles, only one PAM for each joint may reduce the complexity in structure and control of the robotic exoskeleton for now. The designed low-cost, lightweight, and portable upper-limb exoskeleton weighs 5.6 kg, and it is enough to assist patients suffering from high stiffness in upper limb flexor muscles to take frequent intensive rehabilitation exercises in the community or at home as shown in Fig. 2(a).

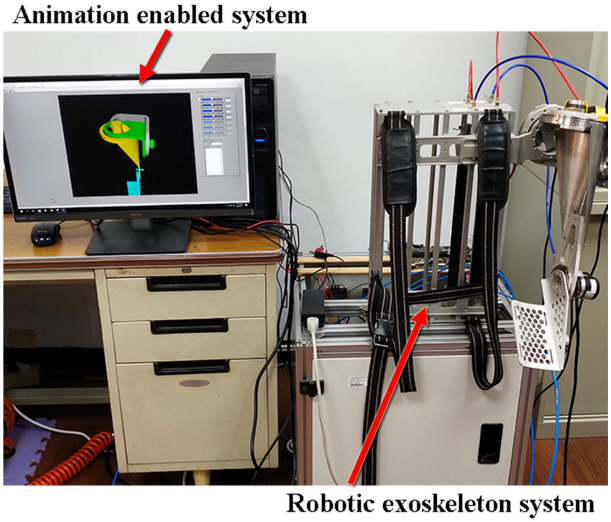

(a)

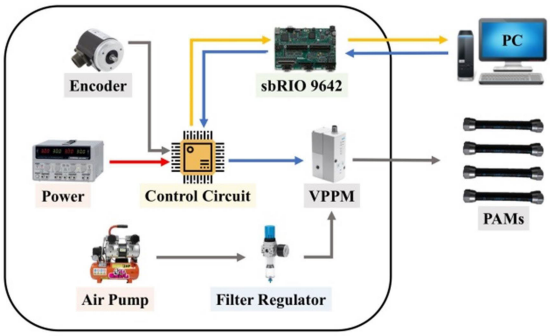

(b)

FIGURE 2. (a) Cable-driven robotic exoskeleton system with PAM actuators as well as the animation enabled system. (b) Control circuit and peripherals.

Moreover, in the developed robotic exoskeleton system a real-time animation is enabled by reading the joint angles to a microcontroller board to animate the graphic model through the Labview development. The animation enabled system featuring synchronicity with the robotic exoskeleton may give a rehabilitation performance evaluation

2) ELECTRONICS DESIGN

A commercially available microcontroller board (NI sbRIO-9632) is used for the main controller. The module NI 9234 in

the board enables the input signal on analog input channel to be buffered, conditioned, and then sampled by a 24-bit Delta-Sigma ADC. The analog output module NI 9263 has four output channels with the specification of 100 kS/s, 16-Bit, ±10 V. The Labview evelopment system is used for the required measurement and control algorithms.

Finally, the actuation unit, peripheral sensor devices and main control board are integrated to the robotic exoskeleton as shown in Fig. 2(b). As the PAMs are filled with the air, the PAMs contract and pull the mechanical load to actuate the upper limb robotic exoskeleton. Instead, by releasing the air from the PAMs and taking advantage of the self-weight of an upper limb the robotic exoskeleton can return to its initial configuration. In this way a rehabilitation exercise can be realized.

III. DYNAMIC MODELING OF UPPER LIMB ROBOTIC EXOSKELETON

A. PAM MODEL

PAMs contract in the axial direction by filling a compressed air into the tube to generate a pulling force. The resulted contractile forces actuate the joints through the cables. The contractile force Fc can be described as linearly proportional to the relative pressure P and a monotonic function of braid angle that varies with the contraction length as depicted in (1) [35], [36]

$$F_c = \pi r_0^2 P[\alpha\,(1-\varepsilon)^2 - \beta], \tag{1}$$

where $\alpha = 3/\tan^2\theta_0$, $\beta = 1/\sin^2\theta_0$, $\varepsilon = (l_0 - l)/l_0 = \Delta l/l_0$, r_0 is the initial radius of the PAM. l_0 and l are the respective initial length and real length of the PAM, whose difference is defined as the contraction length Δl. θ_0 is the initial braid angle of the PAM. The internal pressure of the PAM is controlled by an input voltage to the proportional pneumatic pressure regulator.

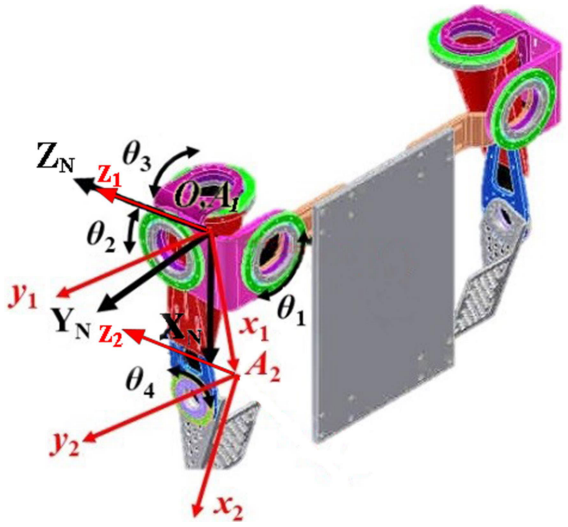

FIGURE 3. Coordinate systems assignment for dynamic formulation.

B. DYNAMIC EQUATIONS INCLUDING PAM ACTUATORS

The basic geometric structure of the robotic exoskeleton for the dynamic formulation is illustrated in Fig. 3, in which an inertial N-frame, $O\_X_NY_NZ_N$, is specified with the Z_N, Y_N, and X_N axis being respectively along the J_1-, J_2-, and J_3-joint axis as referred to the initial configuration, and thus the intersection point of these three joint axes of shoulder is defined as the origin O. The local l_1-frame $\{A_1\_x_1y_1z_1\}$, whose origin is coincident with the point O, is fixed to the upper arm, and the corresponding x1 axis is along the upper arm. The other local coordinate system, l_2-frame $\{A_2\_x_2y_2z_2\}$ with its origin A_2 being at the elbow J_4-joint is attached to the forearm, and its x2 axis is defined along the forearm.

With the defined coordinate systems, let ρ_i $(i = 1, 2)$ be the position vectors from the origin A_i to a differential mass dm_i on the respective upper arm (segment $i = 1$) and forearm (segment $i = 2$) with respect to the corresponding l_i-frame. The position vectors of the differential masses measured with respect to the inertial N-frame can thus be expressed as

$$\boldsymbol{r_1} = {}^N_1\boldsymbol{R}\boldsymbol{\rho_1}, \tag{2}$$

$$\boldsymbol{r_2} = {}^N_1\boldsymbol{R}\boldsymbol{L_1} + {}^N_2\boldsymbol{R}\boldsymbol{\rho_2} = {}^N_1\boldsymbol{R}\,(l_1\boldsymbol{u_1}) + {}^N_2\boldsymbol{R}\boldsymbol{\rho_2}, \tag{3}$$

where ${}^N_i\boldsymbol{R}$ $(i = 1, 2)$ is the rotation matrix describing the coordinate transformation from the l_i-frame to the inertial N-frame. Moreover, in accordance with the joint structure of the proposed robotic exoskeleton, the Z-Y-X Euler angles $\begin{bmatrix}\psi & \theta & \varphi\end{bmatrix}^T$ are better used to specify the orientation of two coordinates, so that the coordinate transformation matrix ${}^j_i\boldsymbol{R}$ from the l_i-frame to the l_j-frame is represented as

$${}^j_i\boldsymbol{R} = \begin{bmatrix} c\psi c\theta & -s\psi c\varphi + c\psi s\theta s\varphi & s\psi s\varphi + c\varphi s\theta c\varphi \\ s\psi c\theta & c\psi c\varphi + s\psi s\theta s\varphi & -c\psi s\varphi + s\psi s\theta c\varphi \\ -s\theta & c\theta s\varphi & c\theta c\varphi \end{bmatrix}, \tag{4}$$

where "c" stands for cosine, and "s" stands for sine.

In addition, $\boldsymbol{L_i} = l_i\boldsymbol{u_i}$ with the length l_i denotes the length vectors of the segment i with respect to the l_i-frame, and $\boldsymbol{u_i}$ is the unit vector along the corresponding arm axis and expressed in the l_i-frame.

The absolute velocities of the differential masses on each arm are given by taking the derivatives on Eqs. (2) (3) as

$$\dot{\boldsymbol{r}}_1 = {}^N_1\boldsymbol{R}\tilde{\boldsymbol{\omega}}_1\boldsymbol{\rho_1}, \tag{5}$$

$$\dot{\boldsymbol{r}}_2 = {}^N_1\boldsymbol{R}\tilde{\boldsymbol{\omega}}_1\boldsymbol{L_1} + {}^N_2\boldsymbol{R}\tilde{\boldsymbol{\omega}}_2\boldsymbol{\rho_2}, \tag{6}$$

where the time derivative of a rotation matrix ${}^N_i\boldsymbol{R}$ is defined as

$${}^N_i\dot{\boldsymbol{r}} = {}^N_i\boldsymbol{R}\tilde{\boldsymbol{\omega}}_i, \quad (i = 1, 2) \tag{7}$$

Moreover, the tilde over a vector $\tilde{\boldsymbol{\omega}}_i$ denotes a skew symmetric matrix formed from the vector $\boldsymbol{\omega_i}$ that is the absolute angular velocity of the segment i of the arm with respect to the l_i-frame, and is expressed as

$$\tilde{\boldsymbol{\omega}} = \begin{bmatrix} 0 & -\omega_z & \omega_y \\ \omega_z & 0 & -\omega_x \\ -\omega_y & \omega_x & 0 \end{bmatrix}, \tag{8}$$

According to a rigid body motion, the total kinetic energy of the robotic exoskeleton including the wearer's arm is expressed in a matrix-vector form as

$$T = \frac{1}{2}\sum_{i=1}^{2}\int \dot{\boldsymbol{r}}_i^T \dot{\boldsymbol{r}}_i dm_i = \frac{1}{2}\boldsymbol{\omega}_1^T \boldsymbol{I}_1 \boldsymbol{\omega}_1 + \frac{1}{2} m_2 \boldsymbol{\omega}_1^T \tilde{\boldsymbol{L}}_1^T \tilde{\boldsymbol{L}}_1 \boldsymbol{\omega}_1 + m_2 \boldsymbol{d}_2^T \tilde{\boldsymbol{\omega}}_2{}^T {}_2^N \boldsymbol{R}^T {}_1^N \boldsymbol{R} \tilde{\boldsymbol{\omega}}_1 \boldsymbol{L}_1 + \frac{1}{2}\boldsymbol{\omega}_2^T \boldsymbol{I}_2 \boldsymbol{\omega}_2, \quad (9)$$

where m_i is mass of the arm i ($i = 1, 2$), $\boldsymbol{I}_i = \int \tilde{\rho}_i^T \tilde{\rho}_i \mathrm{d}m_i$ denotes the mass moment of inertia matrix about $\mathrm{A_i}$ in the $\mathrm{l_i}$-frame, and $\boldsymbol{d}_i$ specifies the position vector of the gravity center of the segment i, being expressed in the $\mathrm{l_i}$_frame.

On the assumption that the origin of the N-frame is chosen as the zero reference of the gravitational potential energy, the total potential energy is represented as

$$V = \sum_{i=1}^{2}(-\boldsymbol{g}^T \boldsymbol{r}_i dm_i) = -m_1 \boldsymbol{g}^T {}_1^N \boldsymbol{R} \boldsymbol{d}_1 - m_2 \boldsymbol{g}^T {}_1^N \boldsymbol{R} \boldsymbol{L}_1 - m_2 \boldsymbol{g}^T {}_2^N \boldsymbol{R} \boldsymbol{d}_2, \quad (10)$$

where the gravity $\boldsymbol{g}$ is introduced for the potential energy.

It is seen that the kinetic and potential energies are expressed in matrix forms as the function of quasi-velocities and rotation matrices. Substituting Eqs. (9)(10) into the Lagrange formulation in terms of quasi coordinates [37], [38] for the development of dynamic equations,

$$\frac{d}{dt}\left(\frac{\partial T}{\partial \boldsymbol{\omega}_i}\right) + \tilde{\boldsymbol{\omega}}_i \frac{\partial T}{\partial \boldsymbol{\omega}_i} - \frac{\partial T}{\partial {}_i^N \boldsymbol{R}} + \frac{\partial V}{\partial {}_i^N \boldsymbol{R}} = \boldsymbol{Q}_i, \quad (11)$$

along with the following useful identities for symbolic computations

$$\frac{\partial}{\partial \boldsymbol{R}}\left(\boldsymbol{a}^T \boldsymbol{R} \boldsymbol{b}\right) = \tilde{\boldsymbol{b}} \boldsymbol{R}^T \boldsymbol{a}, \quad (12)$$

$$\tilde{\boldsymbol{a}} \tilde{\boldsymbol{b}} \boldsymbol{c} = (\tilde{\boldsymbol{b}} \tilde{\boldsymbol{c}}^T + \tilde{\boldsymbol{c}} \tilde{\boldsymbol{b}}) \boldsymbol{a}, \quad (13)$$

The dynamic equations were derived in a closed form as

$$\begin{bmatrix} \boldsymbol{I}_1 + m_2 \tilde{\boldsymbol{L}}_1^T \tilde{\boldsymbol{L}}_1 & m_2 \tilde{\boldsymbol{L}}_1^T {}_1^2 \boldsymbol{R} \tilde{\boldsymbol{d}}_2 \\ m_2 \tilde{\boldsymbol{d}}_2^T {}_1^2 \boldsymbol{R} \tilde{\boldsymbol{L}}_1 & \boldsymbol{I}_2 \end{bmatrix} \begin{bmatrix} \dot{\boldsymbol{\omega}}_1 \\ \dot{\boldsymbol{\omega}}_2 \end{bmatrix} + \begin{bmatrix} \tilde{\boldsymbol{\omega}}_1 \boldsymbol{I}_1 + m_2 \tilde{\boldsymbol{L}}_1^T \tilde{\boldsymbol{L}}_1 & \boldsymbol{0} \\ \boldsymbol{0} & \boldsymbol{\omega}_2 \boldsymbol{I}_2 \end{bmatrix} \begin{bmatrix} \boldsymbol{\omega}_1 \\ \boldsymbol{\omega}_2 \end{bmatrix} + \begin{bmatrix} -m_1 \tilde{\boldsymbol{d}}_1 {}_1^N \boldsymbol{R}^T \boldsymbol{g} - m_2 \tilde{\boldsymbol{L}}_1 {}_1^N \boldsymbol{R}^T \boldsymbol{g} \\ -m_2 \tilde{\boldsymbol{d}}_2 {}_2^N \boldsymbol{R}^T \boldsymbol{g} \end{bmatrix} = \begin{bmatrix} \boldsymbol{Q}_1 \\ \boldsymbol{Q}_2 \end{bmatrix}, \quad (14)$$

or in an abbreviated form

$$\begin{bmatrix} \overline{\boldsymbol{M}}_{11} & \overline{\boldsymbol{M}}_{12} \\ \overline{\boldsymbol{M}}_{21} & \overline{\boldsymbol{M}}_{22} \end{bmatrix} \begin{bmatrix} \dot{\boldsymbol{\omega}}_1 \\ \dot{\boldsymbol{\omega}}_2 \end{bmatrix} + \begin{bmatrix} \overline{H}_{11} & \overline{H}_{12} \\ \overline{H}_{21} & \overline{H}_{22} \end{bmatrix} \begin{bmatrix} \boldsymbol{\omega}_1 \\ \boldsymbol{\omega}_2 \end{bmatrix} + \begin{bmatrix} \overline{\boldsymbol{G}}_1 \\ \overline{\boldsymbol{G}}_2 \end{bmatrix} = \begin{bmatrix} \boldsymbol{Q}_1 \\ \boldsymbol{Q}_2 \end{bmatrix}, \quad (15)$$

where the generalized forces $\boldsymbol{Q}_i$ are designated in terms of the virtual work with

$$\delta w_i = \delta \boldsymbol{\beta}_i^T \boldsymbol{Q}_i, \quad (16)$$

and the associated quasi-coordinates $\boldsymbol{\beta}_i$ are defined in a differential form as $\boldsymbol{\omega}_i = d\boldsymbol{\beta}_i/dt$. This dynamic form (15) that is expressed in terms of quasi-velocities keeps compact, straightforward and well-structured. However, the equations cannot be directly integrated to the generalized coordinates for a model-based controller design and simulation, a velocity transformation relating quasi-velocities to time derivative of angular orientation coordinates such as Euler angles is required.

Making use of the velocity transform matrix $\boldsymbol{C}_i$ relating the absolute quasi-velocity $\boldsymbol{\omega}_i$ and the absolute Euler angular velocity $\dot{\boldsymbol{\gamma}}_i$, the velocity transformation is expressed as

$$\boldsymbol{\omega}_i = \boldsymbol{C}_i \dot{\boldsymbol{\gamma}}_i, \quad (17)$$

Furthermore, the velocity transformation for the relative quasi-velocity $\boldsymbol{\Omega}_i$ and the relative Euler angular velocity $\dot{\boldsymbol{\eta}}_i$ with respect to its preceding segment i-1 is written as

$$\boldsymbol{\Omega}_i = \boldsymbol{D}_i \dot{\boldsymbol{\eta}}_i, \quad (18)$$

where $\boldsymbol{D}_i$ means the relative velocity transform matrix.

Since the upper limb robotic exoskeleton is regarded as a joint type of manipulator, the angular velocities of segment i are equal to that of segment i-1 plus relative components caused by rotational velocities at joint i, and therefore can be written in terms of $\mathrm{l_i}$-frame as

$$\boldsymbol{\omega}_i = {}_{i-1}^{i}\boldsymbol{R} \boldsymbol{\omega}_{i-1} + \boldsymbol{\Omega}_i = {}_{i-1}^{i}\boldsymbol{R} \boldsymbol{\omega}_{i-1} + \boldsymbol{D}_i \dot{\boldsymbol{\eta}}_i, \quad (19)$$

Changing the subscript of Eq. (17) into i-1 and then substituting into the above, a virtual displacement relationship between in the quasi-coordinates and in the joint angles is obtained as

$$\delta \boldsymbol{\beta}_i = {}_{i-1}^{i}\boldsymbol{R} \boldsymbol{C}_{i-1} \delta \boldsymbol{\gamma}_{i-1} + \boldsymbol{D}_i \delta \boldsymbol{\eta}_{i-1}, \quad (20)$$

Also taking the derivative over Eq. (19) leads to the quasi-acceleration as

$$\dot{\boldsymbol{\omega}}_i = {}_{i-1}^{i}\boldsymbol{R} \dot{\boldsymbol{\omega}}_{i-1} + \tilde{\boldsymbol{\omega}}_{i\,i-1}^{i} \boldsymbol{R} \boldsymbol{\omega}_{i-1} + \boldsymbol{D}_i \ddot{\eta}_i + \dot{\boldsymbol{D}}_i \dot{\boldsymbol{\eta}}_i, \quad (21)$$

In order to further transform the dynamic equation (15) to the expression in the joint angles, the virtual work principle for any instantaneous motion was applied to Eq. (15), so that

$$\delta w = \sum_{i=1}^{2} \delta \boldsymbol{\beta}_i^T [\sum_{j=1}^{2} (\overline{\boldsymbol{M}}_{ij} \dot{\boldsymbol{\omega}}_j + \overline{H}_{ij} \boldsymbol{\omega}_j) + \overline{\boldsymbol{G}}_i - \boldsymbol{Q}_i] = 0, \quad (22)$$

Because the segment $i = 0$ is a fixed base, the absolute and relative kinematics characteristics of the segment $i = 1$ are coincident. Based on the Z-Y-X Euler angle transformation,

$$\boldsymbol{\gamma}_1 = \boldsymbol{\eta}_1 = \begin{bmatrix} \theta_1 & \theta_2 & \theta_3 \end{bmatrix}^T, \quad (23)$$

$$\boldsymbol{C}_1 = \boldsymbol{D}_1 = \begin{bmatrix} -s\theta_2 & 0 & 1 \\ c\theta_2 s\theta_3 & c\theta_3 & 0 \\ c\theta_2 c\theta_3 & -s\theta_3 & 0 \end{bmatrix}, \quad (24)$$

And at the elbow joint, only the joint angle θ_4 is designated, that is,

$$\boldsymbol{\eta}_2 = \begin{bmatrix} 0 & \theta_4 & 0 \end{bmatrix}^T, \quad (25)$$

$$\boldsymbol{D_2} = \begin{bmatrix} -s\theta_4 & 0 & 1 \\ 0 & 1 & 0 \\ c\theta_4 & 0 & 0 \end{bmatrix}, \tag{26}$$

and thus

$$\boldsymbol{\Omega_2} = \boldsymbol{D_2}\dot{\boldsymbol{\eta}}_{\boldsymbol{2}} = \dot{\boldsymbol{\theta}}_4 \boldsymbol{v_2}, \tag{27}$$

where $\boldsymbol{v_2} = \begin{bmatrix} 0 & 1 & 0 \end{bmatrix}^T$ is the unit vector along the y_2-axis.

Substituting Eqs. (19)(21) for the respective quasi-velocities and quasi-accelerations and Eq. (20) for the virtual displacements in the quasi-coordinates into Eq. (22), together with the above facts (23-27) for our proposed upper limb robotic exoskeleton design, with any virtual displacement variations in joint angles $\delta\boldsymbol{\theta} = [\delta\theta_1 \ldots \delta\theta_4]$, the equations of motion in (15) are rewritten in terms of the designated joint angles as

$$\boldsymbol{M}\ddot{\boldsymbol{\theta}} + \boldsymbol{H}\dot{\boldsymbol{\theta}} + \boldsymbol{G} = \boldsymbol{\tau}, \tag{28}$$

where $\boldsymbol{\theta} = [\theta_1\theta_2\theta_3\theta_4]^T$ is the joint angle vector for the shoulder joints and elbow joint of the exoskeleton. The inertia matrix $\boldsymbol{M}$ is symmetric and positive definite, $\boldsymbol{H}\dot{\boldsymbol{\theta}}$ is the Coriolis and centrifugal vector, $\boldsymbol{G}$ is the gravity vector, the closed and detailed definitions are fully presented in the followings.

$$\begin{aligned}
\boldsymbol{M_{11}} &= \boldsymbol{C_1^T}\left(\overline{\boldsymbol{M}}_{\boldsymbol{11}} + \overline{\boldsymbol{M}}_{\boldsymbol{12}}{}^{\boldsymbol{2}}_{\boldsymbol{1}}\boldsymbol{R} + {}^{\boldsymbol{1}}_{\boldsymbol{2}}\boldsymbol{R}\overline{\boldsymbol{M}}_{\boldsymbol{21}} + {}^{\boldsymbol{2}}_{\boldsymbol{1}}\boldsymbol{R}^{\boldsymbol{T}}\overline{\boldsymbol{M}}_{\boldsymbol{22}}{}^{\boldsymbol{2}}_{\boldsymbol{1}}\boldsymbol{R}\right)\boldsymbol{C_1}, \\
\boldsymbol{M_{12}} &= \boldsymbol{C_1^T}(\overline{\boldsymbol{M}}_{\boldsymbol{12}} + {}^{\boldsymbol{2}}_{\boldsymbol{1}}\boldsymbol{R}^{\boldsymbol{T}}\overline{\boldsymbol{M}}_{\boldsymbol{22}})\boldsymbol{v_2}, \\
\boldsymbol{M_{21}} &= \boldsymbol{v_2^T}(\overline{\boldsymbol{M}}_{\boldsymbol{21}} + \overline{\boldsymbol{M}}_{\boldsymbol{22}}{}^{\boldsymbol{2}}_{\boldsymbol{1}}\boldsymbol{R})\boldsymbol{C_1}, \\
\boldsymbol{M_{22}} &= \boldsymbol{v_2^T}\overline{\boldsymbol{M}}_{\boldsymbol{22}}\boldsymbol{v_2}, \\
\boldsymbol{H_{11}} &= \boldsymbol{C_1^T}\left(\overline{\boldsymbol{M}}_{\boldsymbol{11}} + \overline{\boldsymbol{M}}_{\boldsymbol{12}}{}^{\boldsymbol{2}}_{\boldsymbol{1}}\boldsymbol{R} + {}^{\boldsymbol{1}}_{\boldsymbol{2}}\boldsymbol{R}\overline{\boldsymbol{M}}_{\boldsymbol{21}} + {}^{\boldsymbol{2}}_{\boldsymbol{1}}\boldsymbol{R}^{\boldsymbol{T}}\overline{\boldsymbol{M}}_{\boldsymbol{22}}{}^{\boldsymbol{2}}_{\boldsymbol{1}}\boldsymbol{R}\right)\dot{\boldsymbol{C}}_{\boldsymbol{1}} \\
&\quad + \boldsymbol{C_1^T}[\overline{\boldsymbol{H}}_{\boldsymbol{11}} + \dot{\boldsymbol{\theta}}_4(\overline{\boldsymbol{M}}_{\boldsymbol{12}} + {}^{\boldsymbol{2}}_{\boldsymbol{1}}\boldsymbol{R}^{\boldsymbol{T}}\overline{\boldsymbol{M}}_{\boldsymbol{22}})\tilde{\boldsymbol{v}}_{\boldsymbol{2}}{}^{\boldsymbol{2}}_{\boldsymbol{1}}\boldsymbol{R} \\
&\quad + {}^{\boldsymbol{2}}_{\boldsymbol{1}}\boldsymbol{R}^{\boldsymbol{T}}\overline{\boldsymbol{H}}_{\boldsymbol{22}}{}^{\boldsymbol{2}}_{\boldsymbol{1}}\boldsymbol{R}]\boldsymbol{C_1}, \\
\boldsymbol{H_{12}} &= \boldsymbol{C_1^T}{}^{\boldsymbol{2}}_{\boldsymbol{1}}\boldsymbol{R}^{\boldsymbol{T}}\overline{\boldsymbol{H}}_{\boldsymbol{22}}\boldsymbol{v_2}, \\
\boldsymbol{H_{21}} &= \boldsymbol{v_2^T}[\left(\overline{\boldsymbol{M}}_{\boldsymbol{21}} + \overline{\boldsymbol{M}}_{\boldsymbol{22}}{}^{\boldsymbol{2}}_{\boldsymbol{1}}\boldsymbol{R}\right)\dot{\boldsymbol{C}}_{\boldsymbol{1}} + (\dot{\boldsymbol{\theta}}_4\overline{\boldsymbol{M}}_{\boldsymbol{22}}\tilde{\boldsymbol{v}}_{\boldsymbol{2}} + \overline{\boldsymbol{H}}_{\boldsymbol{22}}){}^{\boldsymbol{2}}_{\boldsymbol{1}}\boldsymbol{R}\boldsymbol{C_1}], \\
\boldsymbol{H_{22}} &= \boldsymbol{v_2^T}\overline{\boldsymbol{H}}_{\boldsymbol{22}}\boldsymbol{v_2}, \\
\boldsymbol{G_1} &= \boldsymbol{C_1^T}\left(\overline{\boldsymbol{G}}_{\boldsymbol{1}} + {}^{\boldsymbol{2}}_{\boldsymbol{1}}\boldsymbol{R}^{\boldsymbol{T}}\overline{\boldsymbol{G}}_{\boldsymbol{2}}\right), \\
\boldsymbol{G_2} &= \boldsymbol{v_2^T}\overline{\boldsymbol{G}}_{\boldsymbol{2}},
\end{aligned}$$

Moreover, the property that $(\dot{\boldsymbol{M}} - 2\boldsymbol{H})$ is a skew-symmetric matrix existing in a Lagrange dynamic system leads to the identity

$$\dot{\boldsymbol{M}} = \boldsymbol{H} + \boldsymbol{H}^T, \tag{29}$$

In addition, the joint torque τ_i at the i-th joint is resulted from the contractile force F_i of the PAM i ($i = 1,\ldots 4$) about the joint, and thus can be computed by multiplying the contractile force F_i by the joint radius r_i. The contractile force F_i is controlled by the filled relative pressure P_i that is linearly proportional to the input voltage u_i. Also the contraction length Δl_i of the PAM enables a corresponding joint angle θ_i with $\Delta l_i = r_i\,\theta_i$. The joint torque τ_i is thus represented as

$$\tau_i = r_i\pi r_0^2[\alpha\,(1 - r_i\theta_i/l_0)^2 - \beta]u_i = f_i(\theta_i)u_i, \tag{30}$$

where $f_i\,(\theta_i) = r_i\pi r_0^2[\alpha\,(1 - r_i\theta_i/l_0)^2 - \beta]$ implies a nonlinear function of the joint angles.

The dynamic equations of the upper limb robotic exoskeleton are rewritten after substituting Eq. (30) into Eq. (28) as

$$\boldsymbol{M}\ddot{\boldsymbol{\theta}} + \boldsymbol{H}\dot{\boldsymbol{\theta}} + \boldsymbol{G} = \boldsymbol{B}\boldsymbol{u}, \tag{31}$$

where the input matrix $\boldsymbol{B}$= diag$[f_1 \ldots f_4]$ is positive definite.

When the robotic exoskeleton is used for rehabilitation training, the motion controller must be well designed to track the rehabilitation trajectory to ensure the effectiveness in rehabilitation. However, the designed upper limb robotic exoskeleton may suffer from structural parameter uncertainties, external disturbances like the flexibility of the cable, hysteresis existing on PAMs and cable-driven robot, measured noise, etc., an advanced nonlinear controller is required for the cable-driven robotic exoskeleton. Based on the formulated dynamic equations (31), if some parameter uncertainties $\Delta\boldsymbol{M}$, $\Delta\boldsymbol{H}$, $\Delta\boldsymbol{G}$, $\Delta\boldsymbol{B}$ and external disturbances are assumed to exist in the system, Eq.(31) can be rewritten as

$$\begin{aligned}
\boldsymbol{M}\ddot{\boldsymbol{\theta}} + \boldsymbol{H}\dot{\boldsymbol{\theta}} + \boldsymbol{G} &= \boldsymbol{B}\boldsymbol{u} + \left(-\Delta\boldsymbol{M}\ddot{\boldsymbol{\theta}} - \Delta\boldsymbol{H}\dot{\boldsymbol{\theta}} - \Delta\boldsymbol{G} + \Delta\boldsymbol{B}\boldsymbol{u}\right) \\
&= \boldsymbol{B}\boldsymbol{u} + \boldsymbol{d}(t),
\end{aligned} \tag{32}$$

And an adaptive fuzzy sliding mode control (AFSMC) is proposed for the rehabilitation control of the cable-driven upper limb robotic exoskeleton with PAM actuators.

IV. CONTROL DESIGN

It is well known that sliding mode control (SMC) is an effective technique relative to the parametric uncertainties and external disturbances. A sliding surface must be first defined to specify the desired closed-loop performance. The time-varying sliding surface here is expressed as

$$\boldsymbol{s}\,(\boldsymbol{\theta}) = \dot{\boldsymbol{\theta}} - (\dot{\boldsymbol{\theta}}_{\boldsymbol{d}} - \boldsymbol{\Lambda}\tilde{\boldsymbol{\theta}}) = \dot{\boldsymbol{\theta}} - \dot{\boldsymbol{\theta}}_{\boldsymbol{r}}, \tag{33}$$

in which $\tilde{\boldsymbol{\theta}} = \boldsymbol{\theta} - \boldsymbol{\theta}_{\boldsymbol{d}}$ is the joint angle errors of the robotic exoskeleton. The symmetric positive definite matrix $\boldsymbol{\Lambda}$ is related to the desired performance of the closed-loop system. Moreover, the introduced reference joint rate $\dot{\boldsymbol{\theta}}_{\boldsymbol{r}}$ interprets the sliding surface as the tracking joint rate errors with respect to the reference joint rates.

Conventionally, SMC is composed of the nominal control $\boldsymbol{u_{eq}}$ and the reaching control $\boldsymbol{u_r}$ in the presence of model imprecision or external disturbances. The nominal control $\boldsymbol{u_{eq}}$ can be determined by making the derivative of the sliding surface zero as

$$\boldsymbol{u_{eq}} = \boldsymbol{B}^{-1}(\boldsymbol{M}\ddot{\boldsymbol{\theta}}_{\boldsymbol{r}} + \boldsymbol{H}\dot{\boldsymbol{\theta}}_{\boldsymbol{r}} + \boldsymbol{G}), \tag{34}$$

By the nature, the reaching control $\boldsymbol{u_r}$ expressed in a sign function will excite a chattering and induce the damage to the robotic exoskeleton. To overcome the drawback, some methods were proposed such as the integral type of SMC, incorporated thin boundary layer or a sigmoid function to smooth out the control discontinuity. In this paper the adaptive fuzzy type of reaching control is used to remove the discontinuous control signal.

A. ADAPTIVE FUZZY SLIDING MODE CONTROL DESIGN

The fuzzy type of reaching control for the robotic exoskeleton is expressed as

$$\boldsymbol{u_r} = \boldsymbol{B}^{-1}\boldsymbol{K_r FSMC}\left(\boldsymbol{s}, \dot{\boldsymbol{s}}\right), \tag{35}$$

in which

$$\boldsymbol{K_r FSMC}\left(\boldsymbol{s}, \dot{\boldsymbol{s}}\right) = \left[k_{r(1)} FSMC_1(s_1, \dot{s}_1) \cdots k_{r(n)} FSMC_n(s_n, \dot{s}_n)\right]^T$$

is the fuzzy gain vector with the components $k_{r(i)}FSMC_i(s_i, \dot{s}_i)$. The fuzzy function $FSMC$ maps two normalized inputs $s(t)$, and $\dot{s}(t)$ to the linguistic output. The Mamdani inferred rules with seven fuzzy partitions, NB (Negative Big), NM (Negative Medium), NS (Negative Small), ZO (Zero), PS (Positive Small), PM (Positive Medium) and PB (Positive Big) are used for the fuzzy inference. The membership functions of input and output linguistic variables are defined in Fig. 4. As proposed in [39], the product inference with singleton fuzzification and centroid defuzzification methods were employed for the fuzzy implications. The fuzzy function is normalized as $|FSMC_i(s_i, \dot{s}_i)| \leq 1$, and has been set as $(s_i)(FSMC_i(s_i, \dot{s}_i)) \leq -|s_i|$.

The input-output relationships in the fuzzy inference system are determined from the fuzzy logic IF-THEN rule base. Namely for the i_th rule, $R^{(i)}$::IF $\tilde{x}(t)$ is A_1^i and $\dot{\tilde{x}}(t)$ is A_2^i THEN $FSMC_i$ is B^i, A_1^i and A_2^i are the input fuzzy sets and B^i is the output fuzzy set. The designated fuzzy rules are presented in Table 1.

TABLE 1. Fuzzy rules for FSMC.

$FSMC$	s						
$\dot{s}$	NB	NM	NS	ZE	PS	PM	PB
NB	PB	PB	PB	PB	PM	PS	ZE
PM	PB	PB	PB	PM	PS	ZE	NS
NS	PB	PB	PM	ZE	ZE	NS	NM
ZO	PB	PM	PS	ZE	NS	NM	NB
PS	PM	PS	ZE	ZE	NM	NB	NB
PM	PS	ZE	NS	NM	NB	NB	NB
PB	ZE	NS	NM	NB	NB	NB	NB

Totally, the control input takes the form

$$\begin{aligned}\boldsymbol{u}(t) &= \boldsymbol{u_{eq}}(t) + \boldsymbol{u_r}(t)\\ &= \boldsymbol{B}^{-1}(\boldsymbol{M}\ddot{\boldsymbol{\theta}}_{\boldsymbol{r}} + \boldsymbol{H}\dot{\boldsymbol{\theta}}_{\boldsymbol{r}} + \boldsymbol{G}) + \boldsymbol{B}^{-1}\boldsymbol{K_r FSMC}\left(\boldsymbol{s}, \dot{\boldsymbol{s}}\right),\end{aligned} \tag{36}$$

B. STABILITY ANALYSIS

The robotic exoskeleton system (32) is controlled by fuzzy sliding mode controller (36). A Lyapunov candidate $V(t)$ is chosen as

$$V(t) = \frac{1}{2}\left(\boldsymbol{s}^T\boldsymbol{M}\boldsymbol{s}\right), \tag{37}$$

The stability is analyzed by differentiating (37) as

$$\begin{aligned}&\dot{V}(t)\\ &= \boldsymbol{s}^T\boldsymbol{M}\dot{\boldsymbol{s}} + \frac{1}{2}\left(\boldsymbol{s}^T\dot{\boldsymbol{M}}\boldsymbol{s}\right)\\ &= \boldsymbol{s}^T\boldsymbol{M}\left(\ddot{\boldsymbol{\theta}} - \ddot{\boldsymbol{\theta}}_{\boldsymbol{r}}\right) + \frac{1}{2}\left(\boldsymbol{s}^T\dot{\boldsymbol{M}}\boldsymbol{s}\right)\\ &= \boldsymbol{s}^T\left(\boldsymbol{B}\boldsymbol{u} - \boldsymbol{H}\dot{\boldsymbol{\theta}} - \boldsymbol{G} + \boldsymbol{d}(t) - \boldsymbol{M}\ddot{\boldsymbol{\theta}}_{\boldsymbol{r}}\right) + \frac{1}{2}\left(\boldsymbol{s}^T\dot{\boldsymbol{M}}\boldsymbol{s}\right)\\ &= \boldsymbol{s}^T\left(\boldsymbol{B}\left[\boldsymbol{B}^{-1}\left(\boldsymbol{M}\ddot{\boldsymbol{\theta}}_{\boldsymbol{r}} + \boldsymbol{H}\dot{\boldsymbol{\theta}}_{\boldsymbol{r}} + \boldsymbol{G}\right) + \boldsymbol{B}^{-1}\boldsymbol{K_r FSMC}\left(\boldsymbol{s}, \dot{\boldsymbol{s}}\right)\right]\right.\\ &\quad \left. - \boldsymbol{H}\left(\boldsymbol{s} + \dot{\boldsymbol{\theta}}_{\boldsymbol{r}}\right) - \boldsymbol{G} + \boldsymbol{d}(t) - \boldsymbol{M}\ddot{\boldsymbol{\theta}}_{\boldsymbol{r}}\right) + \frac{1}{2}\left(\boldsymbol{s}^T\dot{\boldsymbol{M}}\boldsymbol{s}\right)\\ &= \boldsymbol{s}^T\left(\boldsymbol{K_r FSMC}\left(\boldsymbol{s}, \dot{\boldsymbol{s}}\right) + \boldsymbol{d}(t)\right)\\ &\leq \sum_{i=1}^{n}\left(|d_i(t)| - k_{r(i)}\right)|s_i|\end{aligned} \tag{38}$$

If $k_{r(i)} > |d_i(t)|$ is chosen such that the reaching condition $\dot{\boldsymbol{V}}(t) < 0$ is always satisfied, the stability proof is completed, and the closed-loop system is guaranteed asymptotically stable.

In FSMC the switching fuzzy gains $k_{r(i)}$ are constants that are larger than the upper bounds of $|d_i(t)|$. However, the switching control gains $k_{r(i)}$ can be further determined dynamically to improve the tracking performance of the robotic exoskeleton. As such, a fuzzy inference system is proposed for $k_{r(i)}$. Seven fuzzy partitions for the two normalized inputs $\tilde{\theta}_i$, $\dot{\tilde{\theta}}_i$ and output $k_{r(i)}$ are denoted. The corresponding membership functions of input and output linguistic variables

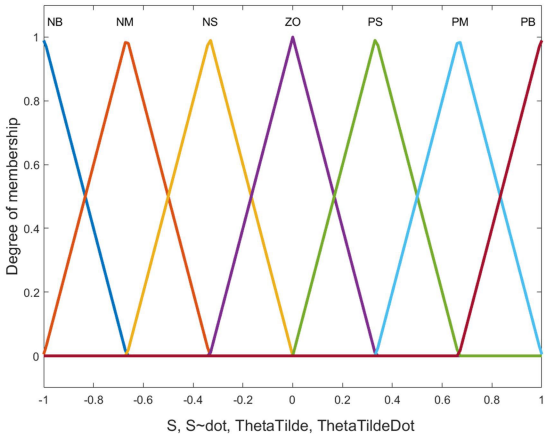

(a)

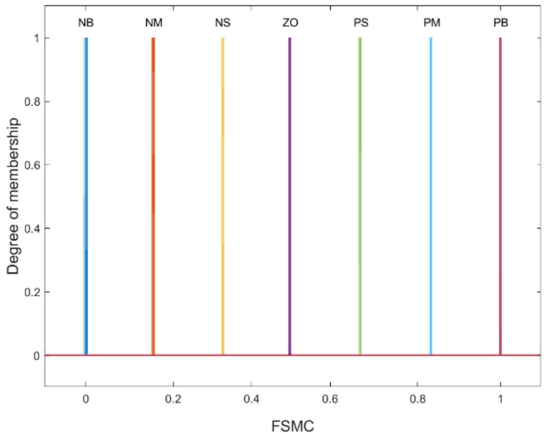

(b)

FIGURE 4. Assigned membership function of the fuzzy sets for (a) input variables (s_i,$\dot{s}_i$), normalized error inputs ($\tilde{\theta}_i$, $\dot{\tilde{\theta}}_i$), and (b) output function $FSMC_i$.

are depicted respectively in Fig. 4(a) and Fig. 5 based on the stability proof and numerous trials. Moreover, the triangular membership functions were used here for its simplicity, computational efficiency and control performance. The fuzzy logic IF-THEN rule base determines the input-output relationships in the fuzzy inference system as shown in Table 2.

TABLE 2. Fuzzy rules for $k_{r(i)}$.

$k_{r(i)}$ / $\tilde{\theta}_i$	$\dot{\tilde{\theta}}_i$						
	NB	NM	NS	ZO	PS	PM	PB
NB	PB	PB	PB	PB	PM	PS	ZO
PM	PB	PB	PB	PM	PS	ZO	NS
NS	PB	PB	PM	ZO	ZO	NS	NM
ZO	PB	PM	PS	ZO	NS	NM	NB
PS	PM	PS	ZO	ZO	NM	NB	NB
PM	PS	ZO	NS	NM	NB	NB	NB
PB	ZO	NS	NM	NB	NB	NB	NB

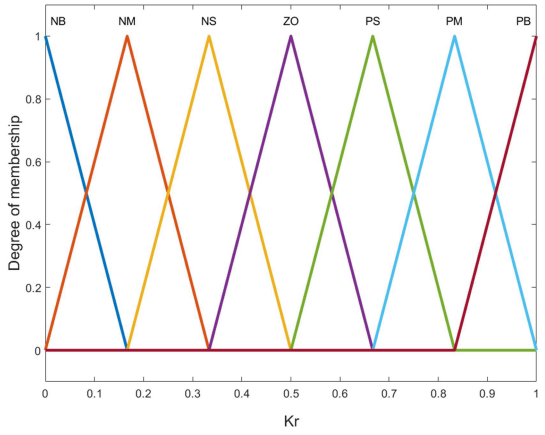

FIGURE 5. Fuzzy sets of switching gain k_r.

Correlation-minimum inference with centroid defuzzification method is used for the fuzzy implications, and thus $k_{r(i)}$ can be adjusted adaptively according to the current joint angle errors and joint rate errors of the robotic exoskeleton.

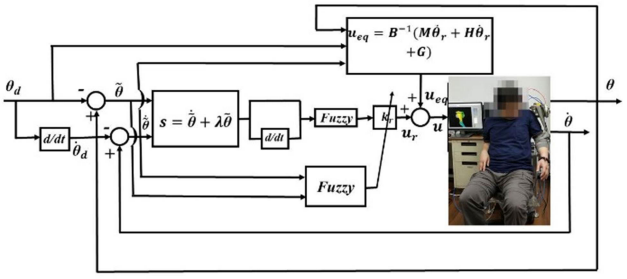

FIGURE 6. Control structure of AFSMC for robotic exoskeleton.

The control structure of the AFSMC for the robotic exoskeleton is shown in Fig. 6. The rehabilitation trajectories are designated by the desired joint angles $\boldsymbol{\theta_d}$. The control signals $\boldsymbol{u}$ for the PAMs are generated by AFSMC, actuating PAMs to produce forces to drive the upper limb robotic exoskeleton to realize a rehabilitation task.

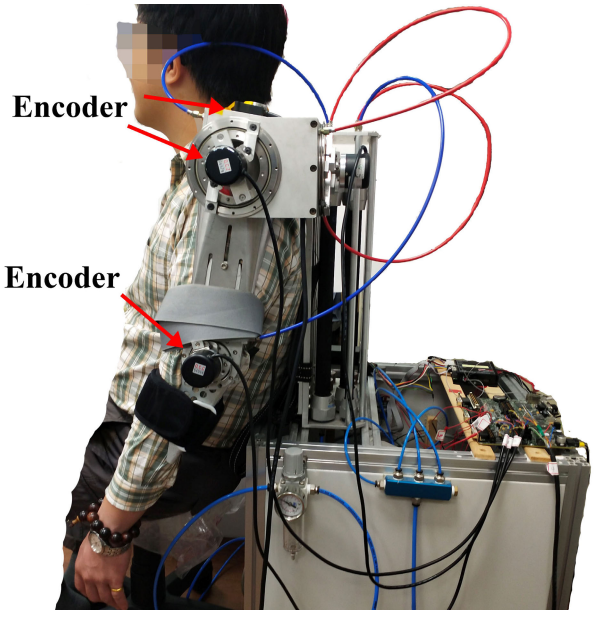

(a)

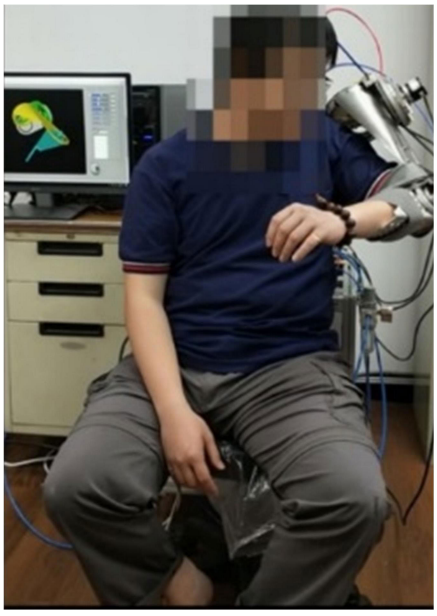

(b)

FIGURE 7. (a) A wearer put on the robotic exoskeleton in an idle posture. (b) A rehabilitation exercise was executed.

V. IMPLEMENTATION AND DISCUSSIONS

As shown in Fig. 7(a)(b), the passive upper-limb rehabilitation exercises were demonstrated by a healthy subject putting on the robotic exoskeleton. The trajectory tracking experiments were conducted to implement rehabilitation motions. The desired trajectories in the joint space were synthesized from the animation enabled system according to the upper limb rehabilitation motions. The parameters of the robotic exoskeleton including the wearer's upper arm and forearm were taken as $m_1 = 1.26$ kg, $m_2 = 0.63$ kg, $\boldsymbol{I_1} = 0.1134$ kg·m^2, $\boldsymbol{I_2} = 0.0252$ kg·m^2, $l_1 = 0.3$ m, $l_2 = 0.2$ m.

The joint radius $r_1 = 0.06$ m, $r_2 = 0.06$ m, $r_3 = 0.06$ m, $r_4 = 0.03$ m. The PAMs in use are $r_0 = 2$cm, $l_0 = 30$cm, $\theta_0 = 25°$, $\alpha = 480$, $\beta = 17.58$.

A. REHABILITATION EXPERIMENT ON JOINTS J1, J2 AND J4

In the first rehabilitation experiment, the rehabilitation trajectories were planned for the shoulder abduction/adduction θ_1, shoulder flexion/extension θ_2, and the elbow flexion/extension θ_4 under the shoulder internal/external rotation $\theta_3 = 0$. The initial pose was defined with his upper arm hung down. Three controllers, PID, FSMC and AFSMC were used and compared on the tracking performance.

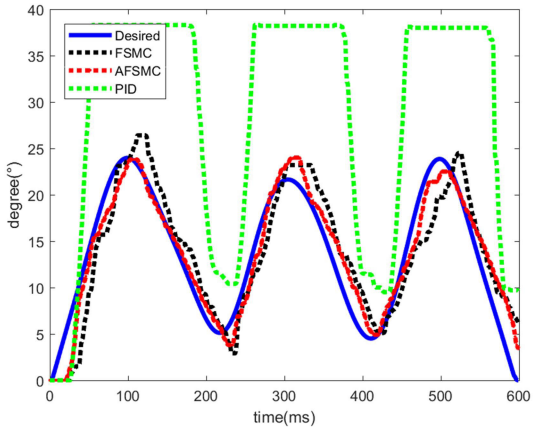

FIGURE 8. Trajectories of shoulder joint J_1.

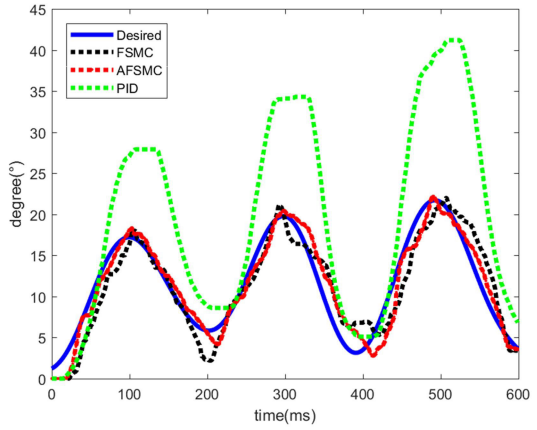

FIGURE 9. Trajectories of shoulder joint J_2.

Figs. 8-10 present the trajectories of the joints J_1, J_2, and J_4 for the three controllers. It is seen that the PID control on trajectory tracking has the worst performance. Especially, there cause very large deviations at the two extreme positions of the rehabilitation cycle because of system uncertainties, nonlinear effects and compressibility of the air. FSMC indeed can suppress the chattering of the conventional SMC design and a better tracking performance can be obtained. In particular, AFSMC apparently has superior tracking performance

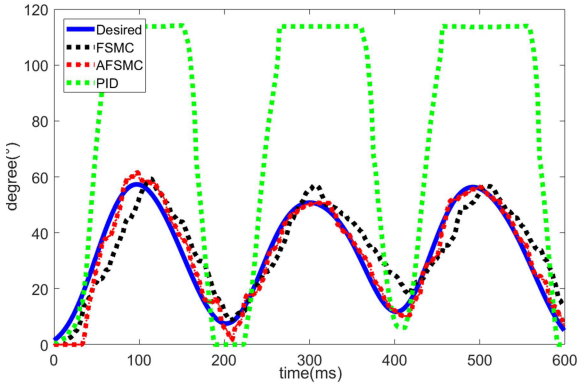

FIGURE 10. Trajectories of shoulder joint J_4.

in rehabilitation tasks by dynamically adjusting the switching fuzzy gains. The corresponding control signals based on AFSMC are presented in Fig. 11.

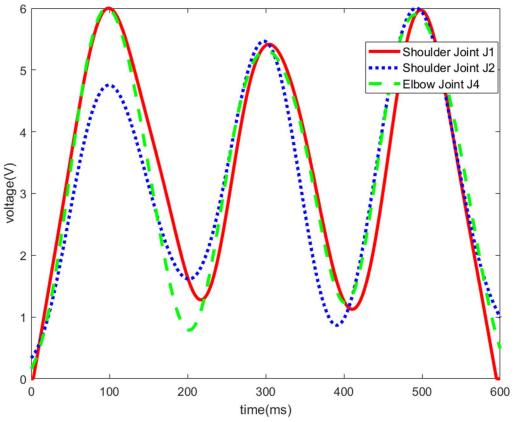

FIGURE 11. Control signals of AFSMC.

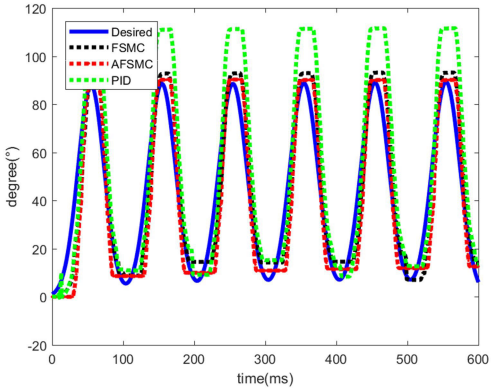

FIGURE 12. Trajectories of shoulder joint J_3.

B. REHABILITATION EXPERIMENT ON JOINTS J3

In the second test, only the shoulder internal/external rehabilitation rotation was specified at the other fixed joint angles $\theta_1 = 40^\circ$, $\theta_2 = 0$, $\theta_4 = 70^\circ$. The trajectories of the joint J_3 for the three controllers are shown in Fig. 12. It can be found that the proposed AFSMC is superior to the other two

controllers for the applications of the robotic exoskeleton to the rehabilitation. Also in the comparison to the first rehabilitation experiment that is a simultaneous multi-joint control, a smooth trajectory tracking can be achieved for the only shoulder internal/external rotation. However, during the repeated shoulder internal/external rotations, it is also revealed that the upper limb is hard to completely return to the initial position only by releasing the air out of a PAM. In this regard, a spring will be required to provide the restoring forces. The control signals for AFSMC are displayed in Fig. 13.

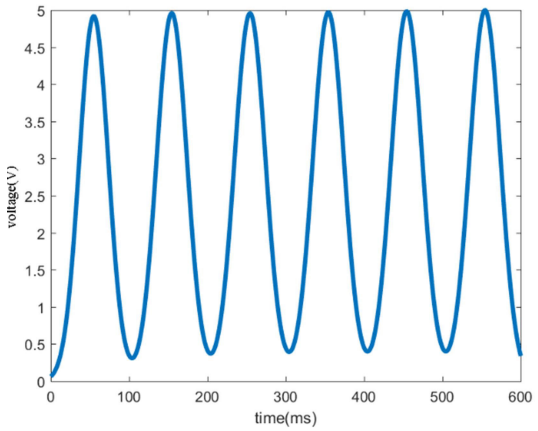

FIGURE 13. Control signals of AFSMC.

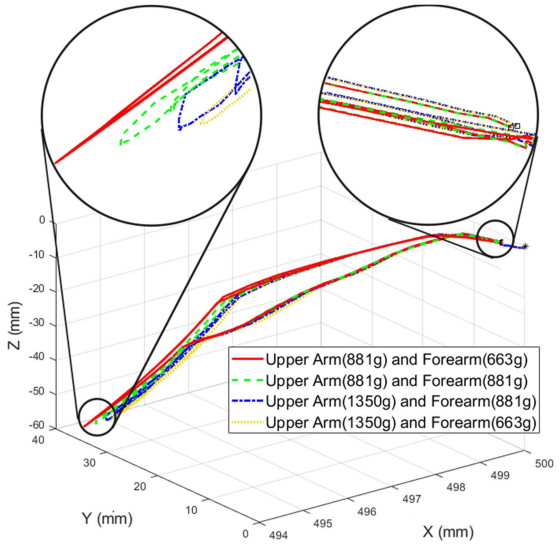

FIGURE 14. Trajectories in the space for different masses by direct command inputs.

Finally, the RMS errors for the three controllers, PID, FSMC, and AFSMC are shown in Table 3. According to Table 3, it can be seen that the RMS errors were statistically and significantly lowered. It is demonstrated that the adaptive nonlinear controller type of AFSMC has a better tracking performance for the developed upper limb robotic exoskeleton.

TABLE 3. Units for magnetic properties.

RMSE	Rehabilitation 1			Rehabilitation 2
	J_1 shoulder joint (θ_1)	J_2 shoulder joint (θ_2)	J_4 elbow joint (θ_4)	J_3 shoulder joint (θ_3)
PID	17.099	10.7635	53.3137	18.8705
FSMC	2.5087	3.5783	8.2311	12.3227
AFSMC	1.7864	2.2606	4.1538	10.4703

C. EFFECT OF DIFFERENT MASSES ON REHABILITATION TRAJECTORIES

In this experiment, different masses were considered for the rehabilitation trajectory. Four combinations of masses were mounted to the upper arm and forearm of the robotic exoskeleton, and the sine signals were commanded to the respective joints J1, J2 and J4. Each rehabilitation task was executed two cycles. The measured joint angles and the associated joint rates, accelerations were then substituted into the forward kinematic equations (3) with $l_1 = 0.25$ m, $l_2 = 0.25$ m to obtain the rehabilitation trajectories in the space. As shown in Fig. 14, the different masses cause the inconsistent trajectories by direct command inputs. Moreover, the larger masses induce larger chattering for the robotic exoskeleton due to the cable-driven design.

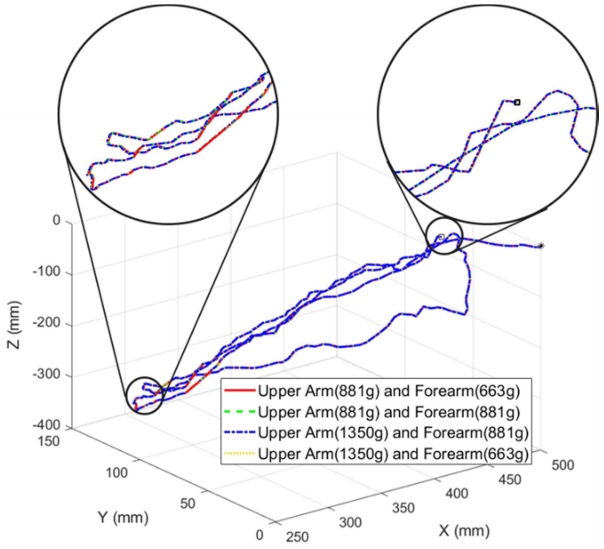

FIGURE 15. Trajectories in the task space for different masses by AFSMC.

The proposed AFSMC was then applied to the rehabilitation exercising for different masses. The desired trajectories in the joint space was specified the same as those in the section 5-1. Following the aforementioned calculations for the forward kinematics, the trajectories in the task space during two cycles are displayed in the Fig. 15. The consistent trajectories show that the AFSMC can effectively eliminate the chattering and is robust to varying masses for rehabilitation applications.

VI. CONCLUSION

To conclude, a new 4-DOF upper limb robotic exoskeleton system was proposed to support shoulder–elbow rehabilitation motion smoothly and reliably. Each joint is driven in one-way actuation by the PAM via a steel cable such that the robotic exoskeleton is characterized with light weight, portability, low cost and safety.

Research efforts were also concentrated on the dynamic modeling and controller design for the reliable implementation of rehabilitation exercises. The dynamic model was developed using the Lagrange formulation in terms of quasi coordinates combined with the virtual work principle. The formulated matrix-vector forms are compact and closed, and feasible for a model based control design. The proposed dynamic modelling can be applied to any other dynamic system without assumptions. Based on the dynamic equations, the model-based AFSMC for the robotic exoskeleton can be designed to effectively realize rehabilitation exercises.

The tracking error analyses conducted by rehabilitation experiment tests have validated the availability of the robotic exoskeleton system on rehabilitation training. Even friction exists between the cable and the conduit, the experimental findings showed that the tension transmission loss in cables occurred only while returning to the initial pose. However, overall performance was adequate for preliminary application of the robotic training for impaired individuals. In the future, a model-free method, such as the active disturbance rejection control (ADRC) could be considered to solve the problem. Also, with the help of clinical trials, it is expected to provide a potential alternative to shoulder–elbow rehabilitation devices, and achieve the rehabilitation training in the community.

REFERENCES

[1] R. A. R. C. Gopura, D. S. V. Bandara, K. Kiguchi, and G. K. I. Mann, "Developments in hardware systems of active upper-limb exoskeleton robots: A review," *Robot. Auto. Syst.*, vol. 75, pp. 203–220, Jan. 2016.

[2] P. Maciejasz, J. Eschweiler, K. Gerlach-Hahn, A. Jansen-Troy, and S. Leonhardt, "A survey on robotic devices for upper limb rehabilitation," *J. Neuroeng. Rehabil.*, vol. 11, no. 1, pp. 1–29, Jan. 2014.

[3] D. Cafolla, M. Russo, and G. Carbone, "CUBE, a cable-driven device for limb rehabilitation," *J. Bionic Eng.*, vol. 16, no. 3, pp. 492–502, May 2019.

[4] J. D. Sanjuan, A. D. Castillo, M. A. Padilla, M. C. Quintero, E. E. Gutierrez, I. P. Sampayo, J. R. Hernandez, and M. H. Rahman, "Cable driven exoskeleton for upper-limb rehabilitation: A design review," *Robot. Auton. Syst.*, vol. 126, pp. 1–25, Apr. 2020.

[5] R. Bogue, "Exoskeletons and robotic prosthetics: A review of recent developments," *Ind. Robot, Int. J.*, vol. 36, no. 5, pp. 421–427, Aug. 2009.

[6] H. Seo and S. Lee, "Design of general-purpose assistive exoskeleton robot controller for upper limbs," *J. Mech. Sci. Technol.*, vol. 33, no. 7, pp. 3509–3519, Jul. 2019.

[7] G. Kwakkel, B. J. Kollen, and H. I. Krebs, "Effects of robot-assisted therapy on upper limb recovery after stroke: A systematic review," *Neurorehabil. Neural Repair*, vol. 22, no. 2, pp. 111–121, Mar. 2008.

[8] C. J. Nycz, T. Butzer, O. Lambercy, J. Arata, G. S. Fischer, and R. Gassert, "Design and characterization of a lightweight and fully portable remote actuation system for use with a hand exoskeleton," *IEEE Robot. Autom. Lett.*, vol. 1, no. 2, pp. 976–983, Jul. 2016.

[9] F. Xiao, Y. Gao, Y. Wang, Y. Zhu, and J. Zhao, "Design and evaluation of a 7-DOF cable-driven upper limb exoskeleton," *J. Mech. Sci. Technol.*, vol. 32, no. 2, pp. 855–864, Feb. 2018.

[10] T. Proietti, V. Crocher, A. Roby-Brami, and N. Jarrasse, "Upper-limb robotic exoskeletons for neurorehabilitation: A review on control strategies," *IEEE Rev. Biomed. Eng.*, vol. 9, pp. 4–14, Apr. 2016.

[11] E. Pirondini, M. Coscia, S. Marcheschi, G. Roas, F. Salsedo, A. Frisoli, M. Bergamasco, and S. Micera, "Evaluation of a new exoskeleton for upper limb poststrokeneuro-rehabilitation: Preliminary results," in *Replace, Repair, Restore, Relieve-Bridging Clinical and Engineering Solutions in Neurorehabilitation*, W. Jensen, O. Andersen, and M. Akay, Eds. New York, NY, USA: Springer, 2014, pp. 637–645.

[12] J. Garrido, W. Yu, and A. Soria, "Modular design and modeling of an upper limb exoskeleton," in *Proc. 5th IEEE RAS/EMBS Int. Conf. Biomed. Robot. Biomechtron.*, São Paulo, Brazil, Aug. 2014, pp. 508–513.

[13] M. A. Ergin and V. Patoglu, "ASSISTON-SE: A self-aligning shoulder-elbow exoskeleton," in *Proc. IEEE Int. Conf. Robot. Autom.*, Saint Paul, MN, USA, May 2012, pp. 2479–2485.

[14] K. Anam and A. A. Al-Jumaily, "Active exoskeleton control systems: State of the art," *Procedia Eng.*, vol. 41, pp. 988–994, Mar. 2012.

[15] Z. Li, C.-Y. Su, G. Li, and H. Su, "Fuzzy approximation-based adaptive backstepping control of an exoskeleton for human upper limbs," *IEEE Trans. Fuzzy Syst.*, vol. 23, no. 3, pp. 555–566, Jun. 2015.

[16] Q. Wu, X. Wang, B. Chen, and H. Wu, "Development of an RBFN-based neural-fuzzy adaptive control strategy for an upper limb rehabilitation exoskeleton," *Mechatronics*, vol. 53, pp. 85–94, Aug. 2018.

[17] H.-B. Kang and J.-H. Wang, "Adaptive control of 5 DOF upper-limb exoskeleton robot with improved safety," *ISA Trans.*, vol. 52, no. 6, pp. 844–852, Nov. 2013.

[18] B. Brahmi, M. Saad, M. H. Rahman, and C. Ochoa-Luna, "Cartesian trajectory tracking of a 7-DOF exoskeleton robot based on human inverse kinematics," *IEEE Trans. Syst., Man, Cybern., Syst.*, vol. 49, no. 3, pp. 600–611, Mar. 2019.

[19] X. C. Zhu, G. L. Tao, B. Yao, and J. Cao, "Adaptive robust posture control of parallel manipulator driven by pneumatic artificial muscles with redundancy," *IEEE/ASME Trans. Mechatronics*, vol. 13, no. 4, pp. 441–450, Aug. 2008.

[20] B. Tondu, "Modelling of the McKibben artificial muscle: A review," *J. Intell. Mater. Syst. Struct.*, vol. 23, no. 3, pp. 225–253, Mar. 2012.

[21] G. Andrikopoulos, G. Nikolakopoulos, and S. Manesis, "Design and development of an exoskeletal wrist prototype via pneumatic artificial muscles," *Meccanica*, vol. 50, no. 11, pp. 2709–2730, Nov. 2015.

[22] X. Tu, X. Zhou, J. Li, C. Su, X. Sun, H. Han, X. Jiang, and J. He, "Iterative learning control applied to a hybrid rehabilitation exoskeleton system powered by PAM and FES," *Cluster Comput.*, vol. 20, no. 4, pp. 2855–2868, Dec. 2017.

[23] C. Xiong, X. Jiang, R. Sun, X. Huang, and Y. Xiong, "Control methods for exoskeleton rehabilitation robot driven with pneumatic muscles," *Ind. Robot, Int. J.*, vol. 36, no. 3, pp. 210–220, May 2009.

[24] Y.-C. Wu, F.-W. Chen, T.-T. Liao, and C.-T. Chen, "Force reflection in a pneumatic artificial muscle actuated haptic system," *Mechatronics*, vol. 61, pp. 37–48, Aug. 2019.

[25] C.-T. Chen, Y.-C. Wu, F.-W. Chen, and M.-Y. Chen, "Pneumatic artificial muscle-driven control loading system (iFUZZY2017)," *Int. J. Fuzzy Syst.*, vol. 20, no. 6, pp. 1779–1789, Aug. 2018.

[26] V. Kvrgic and J. Vidakovic, "Efficient method for robot forward dynamics computation," *Mech. Mach. Theory*, vol. 45, pp. 1–24, Mar. 2020.

[27] S. N. Nabavi, A. Akbarzadeh, and J. Enferadi, "Closed-form dynamic formulation of a general 6-P US robot," *J. Intell. Robot. Syst.*, vol. 96, nos. 3–4, pp. 317–330, Dec. 2019.

[28] S. Pedrammehr, H. Asadi, and S. Nahavandi, "A study on vibrations of hexarot-based High-G centrifugal simulators," *Robotica*, vol. 38, no. 2, pp. 299–316, Feb. 2020.

[29] S. Lu, Y. Li, and B. Ding, "Kinematics and dynamics analysis of the 3PUS-PRU parallel mechanism module designed for a novel 6-DOF gantry hybrid machine tool," *J. Mech. Sci. Technol.*, vol. 34, no. 1, pp. 345–357, 2020.

[30] J. Enferadi and K. Jafari, "A Kane's based algorithm for closed-form dynamic analysis of a new design of a 3RSS-S spherical parallel manipulator," *Multibody Syst. Dyn.*, vol. 49, no. 4, pp. 377–394, Aug. 2020.

[31] Z. E. Kaya and A. Yılmaz, "Modeling and simulation of an anthropomorphic hand prosthesis with an object interaction," *Comput. Meth. Programs Biomed.*, vol. 183, pp. 1–7, Jan. 2020.

[32] S. Cacace, A. C. Lai, and P. Loreti, "Modeling and optimal control of an octopus tentacle," *SIAM J. Control Optim.*, vol. 58, no. 1, pp. 59–84, 2020.

[33] C. Yang, Q. Li, and Q. Chen, "Multi-objective optimization of parallel manipulators using a game algorithm," *Appl. Math. Model.*, vol. 74, pp. 217–243, Oct. 2019.

[34] B. Kim and A. D. Deshpande, "An upper-body rehabilitation exoskeleton harmony with an anatomical shoulder mechanism: Design, modeling, control, and performance evaluation," *Int. J. Robot. Res.*, vol. 36, no. 4, pp. 414–435, Apr. 2017.
[35] C.-J. Lin, C.-R. Lin, S.-K. Yu, and C.-T. Chen, "Hysteresis modeling and tracking control for a dual pneumatic artificial muscle system using Prandtl–Ishlinskii model," *Mechatronics*, vol. 28, pp. 35–45, Jun. 2015.
[36] B. Tondu and P. Lopez, "Modeling and control of McKibben artificial muscle robot actuators," *IEEE Control Syst. Mag.*, vol. 20, no. 2, pp. 15–38, Apr. 2000.
[37] C.-T. Chen and H.-V. Pham, "Trajectory planning in parallel kinematic manipulators using a constrained multi-objective evolutionary algorithm," *Nonlinear Dyn.*, vol. 67, no. 2, pp. 1669–1681, Jan. 2012.
[38] C.-T. Chen and T.-T. Liao, "Trajectory planning of parallel kinematic manipulators for the maximum dynamic load-carrying capacity," *Meccanica*, vol. 51, no. 8, pp. 1653–1674, Aug. 2016.
[39] N. Noroozi, M. Roopaei, and M. Z. Jahromi, "Adaptive fuzzy sliding mode control scheme for uncertain systems," *Commun. Nonlinear Sci. Numer. Simul.*, vol. 14, no. 11, pp. 3978–3992, Nov. 2009.

CHUN-TA CHEN received the B.S. and M.S. degrees in mechanical engineering from National Cheng Kung University, Tainan, Taiwan, in 1985 and 1988, respectively, and the Ph.D. degree in mechanical and aerospace engineering from Case Western Reserve University, Cleveland, OH, USA, in 1996. He is currently a Professor with the Department of Mechatronic Engineering, National Taiwan Normal University, Taipei, Taiwan. His research interests include biologically inspired robots, robotic exoskeletons, and intelligent agricultural harvesting robots.

WEI-YUAN LIEN received the B.S. and M.S. degrees in mechatronic engineering from National Taiwan Normal University, Taipei, Taiwan, in 2015 and 2017, respectively, where he is currently pursuing the Ph.D. degree with the Department of Mechatronic Engineering. His research interests include exoskeleton robots, automatic control on robots, image processing, and machine vision.

CHUN-TING CHEN received the B.S. degree in electrical engineering from Chung Hua University, Hsinchu, Taiwan, in 2009, and the M.S. degree in mechatronic engineering from National Taiwan Normal University, Taipei, Taiwan, in 2013. His research interests include automatic control and robotics.

MING-JENQ TWU received the B.S. degree in mechanical engineering from National Taiwan University and the M.S. and Ph.D. degrees in mechanical engineering from The University of Texas, Arlington, TX, USA. He is currently an Associate Professor with the Department of Mechatronic Engineering, National Taiwan Normal University, Taipei, Taiwan. His research interests include finite element method, robots, and structural analysis.

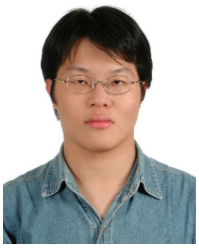

YU-CHENG WU received the B.S. degree in mechanical engineering from National Chung Cheng University, Chiayi, Taiwan, in 2014, and the M.S. degree in mechatronic engineering from National Taiwan Normal University, Taipei, Taiwan, in 2016, where he is currently pursuing the Ph.D. degree with the Department of Mechatronic Engineering. His research interests include exoskeleton robots and automatic control.